J|A|C|S ARTICLES

Published on Web 12/08/2010

Proton Transfer from the Inactive Gas-Phase Nicotine Structure to the Bioactive Aqueous-Phase Structure

Marie-Pierre Gaigeot,*[,†,‡] Alvaro Cimas,[†,▽] Mahamadou Seydou,[§] Ju-Young Kim,[∥] Sungyul Lee,*[,∥] and Jean-Pierre Schermann*[,⊥,#]

Laboratoire Analyse et Modélisation pour la Biologie et l'Environnement, LAMBE UMR8587 CNRS, Université d'Evry val d'Essonne, boulevard F. Mitterrand, Bat. Maupertuis, 91025 Evry Cedex, France, Institut Universitaire de France IUF, 103 boulevard St Michel, 75005 Paris, France, Subatech, Ecole des Mines de Nantes, 4 rue Alfred Kastler, 44307 Nantes, France, Department of Applied Chemistry, Kyunghee University, Kyungki 446-701, South Korea, Department of Biophysics and Biochemical Chemistry, WCU, Seoul National University, Seoul 151-147, South Korea, and Laboratoire de Physique des lasers, CNRS UMR 7538, Institut Galilée, Université Paris 13, Villetaneuse, F-93430, France

Received May 3, 2010; E-mail: mgaigeot@univ-evry.fr; jean-pierre.schermann@univ-paris13.fr; sylee@khu.ac.kr

Abstract: The role of water in the structural change of nicotine from its inactive form in the gas phase to its bioactive form in aqueous solution has been investigated by two complementary theoretical approaches, i.e., geometry optimizations and molecular dynamics. Structures of the lowest-energy nicotine$H^+-(H_2O)_n$ complexes protonated either on the pyridine (inactive form) or pyrrolidine (active form) ring have been calculated, as well as the free-energy barriers for the proton-transfer tautomerization between the two cycles. These structures show chains of 2−4 water molecules bridging the two protonation sites. The room-temperature free-energy barrier to tautomerization along the minimum-energy path from the pyridine to the pyrrolidine cycle drops rapidly when the number of water molecules increases from 0 to 4, but still remains rather high (16 kJ/mol with four water molecules), indicating that the proton transfer is a rather difficult and rare event. We compare results obtained through this explicit water molecule approach to those obtained by means of continuum methods. Car−Parrinello molecular dynamics (CPMD) simulations of the proton-transfer process in bulk with explicit water molecules have been conducted at room temperature. No spontaneous proton transfers have been observed during the dynamics, and biased CPMD simulations have therefore been performed in order to measure the free-energy profile of the proton transfer in the aqueous phase and to reveal the proton-transfer mechanism through water bridges. The MD bias involves pulling the proton from the pyridine ring to the surrounding bulk. Dynamics show that this triggers the tautomerization toward the pyrrolidine ring, proceeding without energy barrier. The proton transfer is extremely fast, and protonation of the pyrrolidine ring was achieved within 0.5 ps. CPMD simulations confirmed the pivotal role played by the water molecules that bridge the two protonation sites of nicotine within the bulk of the surrounding water.

1. Introduction

Despite numerous studies of nicotine prompted by the search for new drugs and the problem of tobacco addiction, the bioactivity of this molecular system still raises questions. Nicotine mimics the effects of the acetylcholine neurotransmitter when binding to brain neuronal acetylcholine receptors (nAChRs).[1] One of the most consistent observations in relation to normal human brain aging is the widespread decline in nicotinic receptors. Nicotine-like ligands are thus widely investigated for the treatment of neurodegenerative disorders, such as the Alzheimer's disease and the Parkinson's disease.[2] Control of pain is also one of the most promising therapeutic applications of nicotine-like drugs.[3] Pharmacophore models, i.e., ensembles of minimal structural features required for the understanding of pharmacological actions, are crucial tools in the search for ligands able to modulate nAChR functions. Beers and Reich[4] proposed the first pharmacophore model of agonists and antagonists compounds at nicotinic junctions. Their model explained specific binding due to the presence of a Coulombic interaction of an onium group and a hydrogen bond acceptor interacting with a receptor-based hydrogen bond donor site. A

[†] Université d'Evry val d'Essonne.
[‡] Institut Universitaire de France.
[§] Ecole des Mines de Nantes.
[∥] Kyunghee University.
[⊥] Seoul National University.
[#] Université Paris 13.
[▽] Present address, Departamento de Quimica e Bioquimica, Facultade de Ciências, Universidade do Porto, Porto, Portugal.

(1) Xiu, X.; Puskar, N. L.; Shanata, J. A. P.; Lester, H. A.; Dougherty, D. A. *Nature* **2009**, *458*, 534.
(2) Romanelli, M. N.; Gratteri, P.; Guandalini, L.; Martini, E.; Bonaccini, C.; Gualtieri, F. *ChemMedChem* **2007**, *2*, 746.
(3) Arneric, S. P.; Holladay, M.; Williams, M. *Biochem. Pharmacol.* **2007**, *74*, 1092.
(4) Beers, W. H.; Reich, E. *Nature* **1970**, *228*, 917.

distance of 4.8 ± 0.3 Å from the onium group N^+ to the hydrogen bond acceptor, such as the pyridine nitrogen atom of nicotine-like agents, was first suggested for bioactivity. Following numerous improvements of this simple pharmacophore model, it was found that active compounds seem in fact to be divided into two classes on the basis of a short (∼4.4 Å) or long (∼5.7 Å) distance. In order to reconcile this somewhat conflicting situation, it has been suggested[5] that a water molecule may hydrogen-bond to the acceptor of the "short-distance" compounds and convert them into "long-distance" compounds, since this water molecule would in turn hydrogen-bond to the receptor.

The role of water thus turns out to be crucial for the bioactivity of nicotine and nicotine-like drugs. Indeed, it has been predicted[6] and recently spectroscopically verified that isolated nicotine is in its inactive form, i.e., protonated on the pyridine ring.[7] In water, the protonation site shifts to the pyrrolidine ring, transforming nicotine into its active form. The hydration state of nicotine and related compounds in the binding sites of the nAChR receptors is most likely neither the one from pure liquid water nor the one from the gas phase, as shown in simulations conducted with rather simple water molecule modeling.[8] Nevertheless, protonation of agonists play a crucial pharmaceutical role in the gating kinetics of the neuronal nicotinic acetylcholine receptor.[9,10]

To the best of our knowledge, the pyridine-to-pyrrolidine proton-transfer tautomerization process of nicotine has not been theoretically characterized, although a first attempt has been published.[7] On the other hand, the tautomerism of the closely related nucleic acid bases has received attention, owing to the importance of mutations in DNA. Hence, numerous geometry optimization studies have been performed in order to investigate the influence of water in the energetic equilibrium between the different base tautomers (a review can be found in ref 11). These calculations include a few explicit water molecules, possibly supplemented by a continuum. Much fewer theoretical studies have been performed to unravel the energetics of the proton-transfer tautomerization process itself. Thorough static calculations for the uracil base in the presence of a few explicit water molecules[12−14] and thymine immersed in implicit solvent[15] have been performed.

Characterizing the proton transfer through static geometry optimizations, including a few explicit water molecules, and exploring the proton-transfer mechanism and energetics in bulk liquid water at room temperature are complementary tasks. The latter has been pioneered by Sagui and co-workers.[16] They performed metadynamics on proton transfer in the model system of formic acid immersed in liquid phase and extracted the free-energy profile of the process, whereas Cucinotta and co-workers considered the keto−enol tautomerization of acetone in solution.[17] Very recent biased molecular dynamics simulations by Tuckerman and co-workers[18] have given access to proton-transfer tautomerization of nucleic acid base pairs in liquid water. In the present work, we investigate the hydration of nicotine and unravel its tautomerization process between inactive and bioactive forms by combining complementary static geometry optimizations and molecular dynamics simulations. In a first step, we progressively add water molecules to isolated nicotine and search for barriers to the proton transfer from the pyridine to the pyrrolidine ring as a function of the number of water molecules. We compare results obtained through this explicit water molecule approach to those obtained by means of continuum methods. In a second step, DFT-based molecular dynamics simulations in the Car−Parrinello framework of the proton-transfer process in bulk with explicit water molecules provide the free-energy profile of the process in aqueous solution.

2. Protonation Site of Isolated Nicotine and Barriers to Tautomerization under Gas-Phase Conditions and in Hydrated Nicotine Complexes

2.1. Theoretical Methods. The density functional theory (DFT) method is employed with the B3LYP/6-311++G(d,p)[19,20] level of theory. Supplementary BLYP/6-311++G(d,p)[19,21] calculations have been done in order to benchmark the BLYP functional that will indeed be used for the dynamics presented in section 3 and is well known for its tendency to underestimate the energetics of H-bonds. Hydrated nicotine complex calculations have been performed with the Gaussian 03 set of programs.[22] Explicit water molecules have been added to nicotineH^+, and the effects of a water continuum have also been investigated using either the IEFPCM method[23] or the COSMO method with the Klamt parametrization,[24] as implemented in Gaussian 03.

Geometry optimizations of nicotineH^+−$(H_2O)_n$ clusters were performed by one-by-one addition of water molecules, from $n = 1$ to 4. We began from nicotineH^+−$(H_2O)_1$, allowing a water molecule to bind to nicotine in a variety of configurations, finding all possible minima on the potential energy surface. We then added another water molecule to nicotine−$(H_2O)_1$, again the additional water molecule being allowed to interact in various ways, finding the most energetically stable structures. We followed this procedure up to nicotineH^+−$(H_2O)_4$. Stationary structures were confirmed by ascertaining that all the harmonic frequencies are real. Structures of transition states (TSs) were obtained by verifying that one and only one of the harmonic frequencies was imaginary and also by carrying out the intrinsic reaction coordinate (IRC) analysis along the reaction

(5) Glennon, R. A.; Dukat, M. *Bioorg. Med. Chem.* **2004**, *14*, 1841.
(6) Graton, J.; Berthelot, M.; Gal, J. F.; Girard, S.; Laurence, C.; Lebreton, J.; Le Questel, J. Y.; Maria, P. C.; Naus, P. *J. Am. Chem. Soc.* **2002**, *124*, 10552.
(7) Seydou, M.; Gregoire, G.; Liquier, J.; Ortega, J. M.; Schermann, J. P.; Desfrancois, C. *J. Am. Chem. Soc.* **2008**, *130*, 4187.
(8) Amiri, S.; Sansom, M.; Biggin, P. *Protein Eng. Des. Sel.* **2007**, *20*, 353.
(9) Elmore, D. E.; Dougherty, D. A. *J. Org. Chem.* **2000**, *65*, 742.
(10) Koné, M.; Illien, B.; Laurence, C.; Gal, J. F.; Maria, P. C. *J. Org. Chem.* **2006**, *19*, 104.
(11) Kabelac, M.; Hobza, P. *Phys. Chem. Chem. Phys.* **2007**, *9*, 903.
(12) Hu, X.; Li, H.; Liang, W.; Han, S. *J. Phys. Chem. B* **2005**, *109*, 5935.
(13) Gutlé, C.; Salpin, J. Y.; Cartailler, T.; Tortajada, J.; Gaigeot, M. P. *J. Phys. Chem. A* **2006**, *110*, 11684.
(14) Li, D.; Ai, H. *J. Phys. Chem. B* **2009**, *113*, 11732.
(15) Fan, J. C.; Shang, Z. C.; Liang, J.; Lui, X. H.; Jin, H. *J. Mol.Struct. THEOCHEM* **2010**, *939*, 106.
(16) Lee, J. G.; Asciutto, E.; Babin, V.; Sagui, C.; Draden, T.; Roland, C. *J. Phys. Chem. B* **2006**, *110*, 2325.
(17) Cucinotta, C. S.; Ruini, A.; Catellani, A.; Stirling, A. *ChemPhysChem* **2006**, *7*, 1229.
(18) Pérez, A.; Tuckerman, M.; Hjalmarson, H. P.; von Lilenfield, O. A. *J. Am. Chem. Soc.* **2010**, *132*, 11510.
(19) Lee, C.; Yang, W.; Parr, R. G. *Phys. Rev. B* **1988**, *37*, 785.
(20) Becke, A. D. *J. Chem. Phys.* **1993**, *98*, 5648.
(21) Becke, A. D. *J. Chem. Phys.* **1992**, *96*, 2155.
(22) Frisch, M. J.; et al. *Gaussian 03*, Revision B03; Gaussian Inc.: Wallingford, CT, 2004.
(23) Tomasi, B.; Mennuci, J.; Cammi, R. *Chem. Rev.* **2005**, *105*, 2999.
(24) Klamt, A.; Jonas, V.; Bürger, T.; Lohrentz, J. C. *J. Phys. Chem. A* **1998**, *102*, 5074.

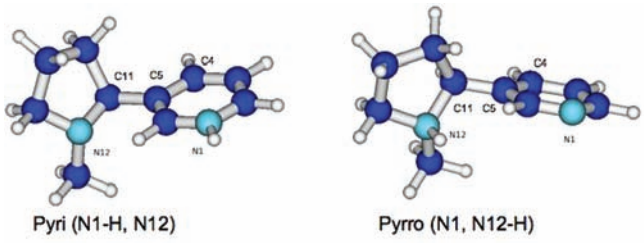

Figure 1. Atom labeling of protonated nicotine used throughout the text. Gas-phase nicotine with protonation at the N1 site (left) and protonation at the N12 site (right). Convention: N, light blue; C, dark blue; H, gray.

pathway. Zero-point energies (ZPE) were taken into account, and default criteria were used for all optimizations.

The proton-transfer process between pyridine and pyrrolidine rings in nicotine$H^+-(H_2O)_{n=1-4}$ clusters was then characterized by transition states. All atoms were allowed to relax freely in the procedure, and thus the calculated barriers were those of the minimum-energy paths. The transition states were confirmed by verifying a single imaginary frequency mode and by carrying out rigorous IRC analyses connecting the reactant, TS, and product. In case the cluster model (which only considers a few solvent molecules directly interacting with nicotineH^+) might underestimate the energy barrier between the two tautomers of nicotine in aqueous solution, we carried out IEFPCM calculations (see Figures 2 and 3 and Supporting Information) including a water continuum surrounding two different nicotine$-(H_2O)_4$ cluster structures. These calculations included stationary- and transition-state structures.

2.2. Results. Nicotine possesses a pyridine and a pyrrolidine ring linked by a C5−C11 bond (Figure 1, the atom numbering convention displayed is identical to that of refs 7 and 25). The orientation of the methyl group of the pyrrolidine cycle with respect to the pyridine cycle is in a *trans* conformation, as previous calculations have shown that the *cis* conformation was sterically unfavorable[9] by 9 kJ/mol.[25] The dihedral angle ψ between the two rings (N12−C11−C5−C4) is the unique structural parameter. The two protonation sites available are the N1 (sp^2) and N12 (sp^3) atoms of the pyridine and pyrrolidine rings, respectively.

Combining geometry optimizations at the *ab initio* level and infrared multiphoton dissociation (IRMPD) experiments, the protonation site of the gas-phase protonated nicotine has been unambiguously attributed to the N1 atom of the pyridine ring, with a resulting conformation that displays a ψ angle between the two rings equal to 165°.[7] This conformation is denoted Pyri-I throughout the text. The two conformations of nicotine protonated at the N12 site of the pyrrolidine ring display $\psi = 289°$ (Pyrro-I) and 115° (Pyrro-II), respectively, and are higher in energy than Pyri-I. Conformation Pyrro-II is more stable than Pyrro-I by 10.2 kJ/mol (see Table 1, B3LYP/6-311++G(d,p) level of calculation).

In the absence of any water molecule, the proton-transfer (tautomerization) process from the pyridine to the pyrrolidine ring requires electronic and free energies (at 298 K) of 305 and 256 kJ/mol, respectively, for a path linking Pyri-I to Pyrro-II. In calculating these values, all atoms are allowed to relax freely, and thus the calculated barriers are those of the minimum-energy paths. This observation indicates that the proton transfer cannot occur under isolated gas-phase conditions, confirming the interpretation of the experimental infrared spectrum of protonated nicotine.[7]

Table 1. Electronic Energy (*E* in Hartree), Zero-Point Energy (ZPE in kJ/mol), Gibbs Free Energy (*G* in Hartree), Relative Energy (ΔE, including ZPE, in kJ/mol), and Relative Gibbs Free Energy (ΔG_{298K} in kJ/mol) of the Lowest-Energy Nicotine$H^+-(H_2O)_n$ Conformers[a]

conformer		*E*	ZPE	G_{298K}	ΔE	ΔG_{298K}
		NicotineH^+				
pyridine	Pyri-I	−499.49652	150.3	−499.05482	0.00	0.00
pyrrolidine	Pyrro-II	−499.49385	151.1	−499.05033	10.2	11.78
		Nicotine$H^+-(H_2O)_1$				
pyridine	pyri-1-a	−575.96944	165.9	−575.48194	30.72	37.28
	pyri-1-b*	−575.98012	165.3	−575.49616	0.00	0.00
	pyri-1-c	−575.97896	165.3	−575.49502	2.92	3.00
pyrrolidine	pyrro-1-1	−575.97589	166.2	−575.48834	14.87	20.52
	pyrro-1-2	−575.96628	166.2	−575.47873	40.29	45.72
	pyrro-1-3	−575.97490	166.2	−575.48793	17.34	21.61
		Nicotine$H^+-(H_2O)_2$				
pyridine	pyri-2-a	−652.455356	181.8	−651.92030	13.80	30.14
	pyri-2-b	−652.457750	180.6	−651.92196	18.26	2.50
	pyri-2-c*	−652.458673	180.6	−651.93178	0.00	0.00
pyrrolidine	pyrro-2-1	−652.460696	182.4	−651.92410	2.46	20.14
	pyrro-2-2	−652.454944	181.7	−651.92358	14.67	21.48
	pyrro-2-3	−652.453776	181.5	−651.92395	16.76	20.53
		Nicotine$H^+-(H_2O)_3$				
pyridine	pyri-3-a	−728.937807	197.5	−728.35607	−1.50	27.88
	pyri-3-b	−728.936771	197.3	−728.35637	0.41	27.08
	pyri-3-c*	−728.934018	195.5	−728.36669	0.00	0.00
pyrrolidine	pyrro-3-1	−728.940306	197.9	−728.35901	−6.31	20.15
	pyrro-3-2	−728.940296	198.2	−728.35736	−5.18	24.49
	pyrro-3-3	−728.936702	197.7	−728.35738	2.38	24.45
		Nicotine$H^+-(H_2O)_4$				
pyridine	pyri-4-a	−805.412164	213.2	−804.78528	8.86	14.12
	pyri-4-b	−805.413472	213.1	−804.78660	5.35	10.66
	pyri-4-c	−805.412675	212.2	−804.79058	3.59	0.20
	pyri-4-d	−805.412153	212.7	−804.78848	6.98	5.72
pyrrolidine	pyrro-4-1	−805.415482	213.8	−804.78760	3.00	8.02
	pyrro-4-2	−805.415162	213.7	−804.78791	3.38	7.23
	pyrro-4-3	−805.412539	213.0	−804.78968	7.27	2.54
	pyrro-4-4*	−805.407906	215.1	−804.79066	0.00	0.00

[a] See Supporting Information. The protonation sites are either on the pyridine (pyri ≡ Pyri-I) or the pyrrolidine ring (pyrro ≡ Pyrro-II). The different pyri conformers are respectively labeled a, b, c, and d. Conformations are respectively labeled pyri-*n*-a, b, c, ... when the protonation site is the pyridine ring and pyrro-*n*-1, 2, 3, ... when the protonation site is the pyrrolidine ring. The asterisks designate the conformers of lowest Gibbs energy taken as reference. All calculations are computed at the B3LYP/6-311++G(d,p) level.

The influence of water molecules on the proton-transfer process is characterized through optimized geometries and transition states of hydrated protonated nicotine$H^+-(H_2O)_n$ complexes, varying the number of water molecules from 1 to 4. The corresponding electronic and free energies of the optimized structures at the B3LYP/6-311++G(d,p) level of theory are reported in Table 1, while structures are depicted in Figures 2 and 3. In these figures, one can also find the optimized transition-state geometries. The relative electronic (ΔE) and free energies (ΔG calculated at 298 K) are also reported. The electronic and free energies (at 298 K) of the barrier for proton transfer from Pyri to Pyrro rings are also reported in the figures ($E^{\ddagger}$ and $G^{\ddagger}$). Additional results obtained with the BLYP functional and continuum models are provided in the Supporting Information. Conformations are respectively labeled pyri-*n*-a, b, c, ... when the protonation site is the pyridine ring and pyrro-*n*-1, 2, 3, ... when the protonation site is the pyrrolidine ring. The corresponding electronic and free energies (at 298 K) are reported in Table 1. Minimum-energy conformations are labeled

(25) Munoz-Caro, C.; Nino, A.; Mora, M.; Reyes, S.; Melendez, F. J.; Castro, M. E. *J. Mol. Struct. THEOCHEM* **2005**, *726*, 115–124.

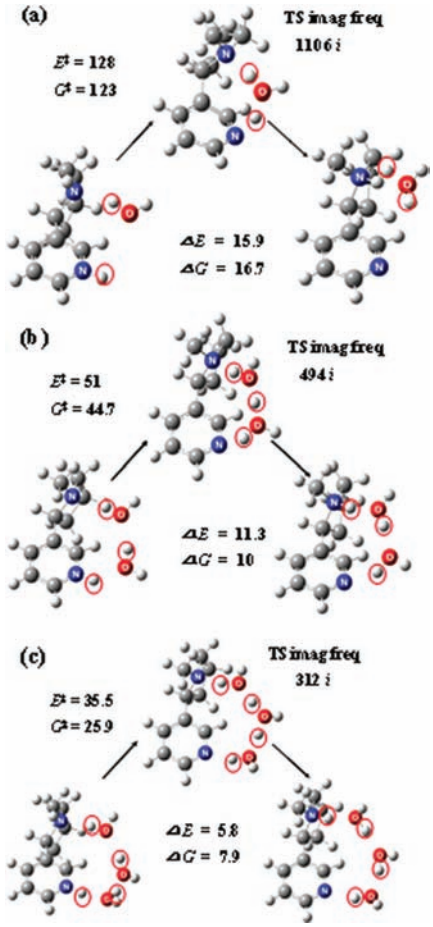

Figure 2. Proton transfer from the pyridine to pyrrolidine site of (a) nicotine$H^+-(H_2O)_1$, (b) nicotine$H^+-(H_2O)_2$, and (c) nicotine$H^+-(H_2O)_3$. Barriers are in kJ/mol. All calculations are computed at the B3LYP/6-311++G(d,p) level. ΔE and ΔG are respectively the electronic- and free-energy (at 298 K) differences between the two stationary optimized geometries. $E^‡$ and $G^‡$ are respectively the electronic and free energy (at 298 K) of the barrier for the proton transfer from pyri (left) to pyrro (right) conformations. The transition states (TS) have been fully optimized (see details in the text). Only the minimum-energy paths for the proton transfer are shown. The imaginary frequencies of the TS are reported. Energies are in kJ/mol. Convention: N, dark blue; C, gray; H, white.

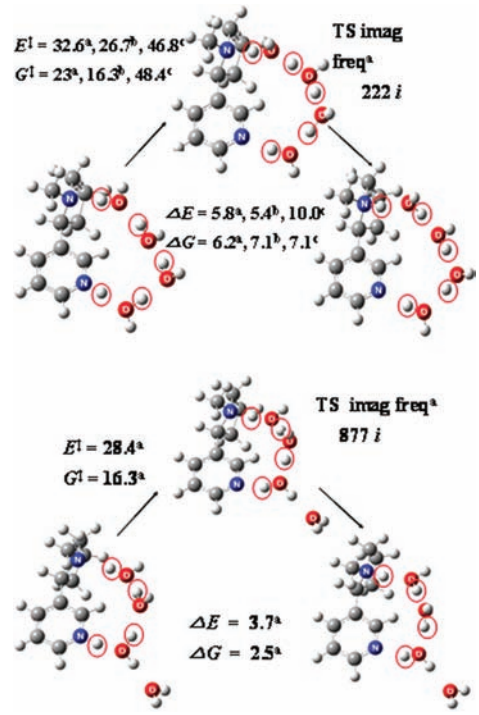

Figure 3. Proton transfer from the pyridine to pyrrolidine site of nicotine$H^+-(H_2O)_4$. Top, four water bridges; bottom, three water bridges. Only the minimum-energy paths for the proton transfer are represented here. [a]B3LYP/6-311++G**, [b]BLYP/6-311++G**, [c]IEFPCM/B3LYP/6-311++G**. ΔE and ΔG are respectively the electronic- and free-energy (at 298 K) differences between the two stationary optimized geometries. $E^‡$ and $G^‡$ are respectively the electronic and free energy (at 298 K) of the barrier for the proton transfer from pyri (left) to pyrro (right) conformations. The transition states (TS) have been fully optimized (see details in the text). Only the minimum-energy paths for the proton transfer are shown. The imaginary frequencies of the TS are reported. Energies are in kJ/mol. Convention: N, dark blue; C, gray; H, white.

with asterisks and have been identified from the minimum in the free energy. Note that the relative electronic-energy order follows the relative free-energy order for all complexes except nicotine$H^+-(H_2O)_3$.

The lowest-energy paths for the proton-transfer tautomerization process of nicotine$H^+-(H_2O)_n$ clusters proceed from pyri-*n*-a to pyrro-*n*-1 conformations. The minimum-energy paths for the proton transfer thus involve pyri conformations that are higher in energy than that of lowest energy. Furthermore, the minimum-energy paths for the proton transfer always lead to the pyrro conformation of lowest energy (i.e., among the pyrro conformations). An illustration providing an understanding of the reason for these results is given in Figure 2a in the case of pyri-1-a. The water molecule, which is H-bonded to the pyrrolidine N12 site in this conformation, is needed for the formation of the pyrro-1-1 conformation of lowest energy (among pyrro structures) once the proton transfer is achieved without involving too much geometrical reorganization. The only exception arises for nicotine$H^+-(H_2O)_4$ when the water molecules can be arranged into "first" and "second" shells around nicotineH^+.

For nicotine$H^+-(H_2O)_1$, the most stable structure (labeled with an asterisk in Table 1) is protonated at the N1 site (pyridine ring). The most stable conformation protonated at the N12 site (pyrrolidine ring) has electronic and free energies respectively 15 and 20.5 kJ/mol above. The lowest-energy barrier for tautomerization corresponds to the proton transfer between conformations pyri-1-a and pyrro-1-1 (Figure 2a). The electronic- and free-energy barriers required for this step are respectively 128 and 123 kJ/mol. In the predicted transition state between these structures, the transferred proton is located on the water molecule to form a hydronium ion (H_3O^+).

As the number of water molecules increases in the nicotine$H^+-(H_2O)_n$ clusters, the energy gap between pyri and pyrro protonated conformers decreases. Following the same trend, the energy barrier to overcome for the proton transfer from the pyridine to the pyrrolidine site becomes significantly smaller (Figures 2 and 3) as the number of water molecules increases. It drops from 128 kJ/mol for one single water molecule down to 51 kJ/mol in the presence of two water molecules and only 35.5 kJ/mol for three water molecules. The corresponding free energies decrease from 123 to 26 kJ/mol.

It is remarkable that the presence of four water molecules complexed to nicotineH^+ is enough to reverse the energy order between pyri and pyrro protonated conformations. Protonation on N12 now provides pyrro conformations of roughly the same free energy as pyri ones. Depending on the arrangement of the four water molecules (a bridge of

four H_2O vs a bridge of three H_2O + one H_2O in a "second" shell", see Figure 3), free energies of 23 and 16 kJ/mol for the proton-transfer tautomerization are obtained with the B3LYP method, and similar but slightly lower barriers are obtained with the BLYP method (Figure 3). Interestingly, when a four-water bridge is formed between the N1 and N12 sites, the energy (and free energy) of the barrier to proton transfer is approximately the same as the one calculated with a three-water bridge. This energy barrier drops further when a single extra water molecule interacts with a three-water bridge. The situation becomes somewhat closer to that of water molecules in the bulk, the extra water molecule then playing the role of the "second hydration layer". Note that a total of four water molecules is probably the maximum number that can be allowed between N1 and N12 due to steric hindrance.

We also considered the effects of a water continuum by employing the COSMO[24] and the IEFPCM methods.[23] Respective energies and optimized structures of the two nicotine tautomers, either neat or embedded into the preceding explicit water complexes, have been obtained from COSMO calculations (see Supporting Information). While the presence of the water continuum significantly modifies the energy differences between tautomers, the water bridges between the two protonation sites are conserved, with only some flips of O−H bonds of the explicit water molecules (see Supporting Information). For the specific case of nicotineH^+−$(H_2O)_4$ complexes, the IEFPCM method has been applied for the proton-transfer pathway (Figure 3). IEFPCM results show that the free-energy barrier for proton transfer is 48 kJ/mol instead of 23 kJ/mol without the continuum.

From the protonated nicotineH^+−$(H_2O)_{1-4}$ complexes, we can infer that increasing the number of water molecules will probably not lead to barriers less than 16 kJ/mol in gas-phase complexes. The second and other hydration layers most probably play an important role and should be taken into account in the modeling. Indeed, adding the continuum representation as a simple modeling of the surrounding bulk led to an increase in the energy of the barrier for the proton transfer. Moreover, thermal fluctuations that are ignored in static hydrated complex calculations play an important role and must also be taken into account. In order to investigate the proton transfer and subsequent tautomerization of nicotine in bulk liquid water at room temperature, molecular dynamics (MD) simulations are the preferred method. For example, simple TIP3P modeling of water molecules has been conducted[26] in classical MD simulations.[27] Quantum mechanical MD allows for more realistic and accurate simulations of proton transfers in liquid water[16,18,28,29] or in solids.[30] We have, therefore, investigated the proton transfer between the two rings of the nicotineH^+ molecule when it is immersed in liquid water by using DFT-based MD simulations in the Car−Parrinello framework, with solute and solvent treated at the same theoretical level. We have extracted the mechanisms and free-energy profile of the proton transfer, which is described in section 3.

3. Dynamics of Proton Transfer in NicotineH^+ Immersed in Liquid Water

The DFT-based Car−Parrinello molecular dynamics (CPMD) method and setup are detailed in section 3.1. Briefly, microcanonical and biased CPMD have been performed in the present work. The microcanonical dynamics provide the overall geometrical features of the solute when immersed in bulk liquid water, i.e., the average relative orientation of the two cycles of the molecule (characterized by ψ angle), and the geometrical organization of the water solvent around the solute in terms of the hydrogen-bonding network formed between the hydrophilic groups of nicotineH^+ and the water molecules, depending on the conformation of the solute (pyri versus pyrro conformations). Biased CPMD simulations have the specific purpose to investigate the proton-transfer mechanism and free-energy profile in the liquid phase.

3.1. Theoretical Methods. The present DFT-based CPMD simulations follow the general setup of our previous simulations.[31−34] All simulations were carried out with the CPMD package.[35] All molecules, i.e., solute and solvent, were explicitly represented. We used the Becke, Lee, Yang, and Parr (BLYP) gradient-corrected functional[19,20] for the exchange and correlation terms. The one-electron orbitals were expanded in a plane-wave basis set with a kinetic energy cutoff of 70 Ry, restricted to the Γ point of the Brillouin zone. Medium soft norm-conserving pseudopotentials of the Martins−Troullier type[36] were used. The core−valence interaction in C, N, and O was treated by s and p potentials with pseudization radii of 1.23, 1.12, and 1.05 au, respectively (taking the same radius for s and p), whereas H atoms were treated as an s potential with a 0.5 au radius. Energy expectation values were calculated in reciprocal space using the Kleinman−Bylander transformation.[37] Dynamics have been performed in the microcanonical ensemble (at constant volume and internal energy) using a fictitious electron mass of 500 au, a time step of 5 au, and periodic boundary conditions applied to a cubic box length of 15 Å. The volume and number of molecules in the box were chosen in order to provide a density of liquid water of 1 g/cm^3, together with sufficient layers of water surrounding the solute. The resultant pressure has not been calculated. We ensured that both the volume of the box and the number of water molecules occupying that volume were correct by careful inspection of radial distribution functions. The water box was initially equilibrated with the TIP3P classical force field for 100 ps (using our homemade MDVRY program[38]). The protonated nicotine solute was then inserted at the center of the box (substituting water molecules that occupy the same space), and the nicotineH^+−liquid water system was subsequently equilibrated within the CPMD setup for 10 ps. This was followed by data collection over strictly microcanonical trajectories of 12−15 ps. Separate dynamics were performed, depending on the protonation site of the nicotine solute: protonation at the pyridine ring

(26) Schmidt, R. G. *Solid State Ionics* **1995**, *77*, 3.
(27) Friedmann, R.; Nachliel, E. M. G. *Biochim. Biophys. Acta* **2005**, *171*, 67.
(28) Marx, D.; Tuckermann, M.; Parrinello, M. *Nature* **1999**, *397*, 601.
(29) Doltsinis, N. L.; Sprik, M. *Phys. Chem. Chem. Phys.* **2003**, *5*, 2612.
(30) Dopieralski, P.; Panek, J.; Latajka, Z. *J. Chem. Phys.* **2009**, *130*, 164517.
(31) Gaigeot, M. P.; Sprik, M. *J. Phys. Chem B* **2004**, *108*, 7458.
(32) Gaigeot, M. P.; Sprik, M. *J. Phys. Chem B* **2003**, *107*, 10344.
(33) Gregoire, G.; Gaigeot, M. P.; Marinica, D. C.; Lemaire, J.; Schermann, J. P.; Desfrançois, C. *Phys. Chem. Chem. Phys.* **2007**, *9*, 3082.
(34) Marinica, D. C.; Gregoire, G.; Desfrancois, C.; Schermann, J. P.; Borgis, D.; Gaigeot, M. P. *J. Phys. Chem. A* **2006**, *110*, 8802.
(35) *CPMD*; International Business Machines Corp., 1990−2008 and Max Planck Institute fuer Festkoerperforschung, Stuttgart, 1995−2001.
(36) Troullier, N.; Martins, J. L. *Phys. Rev. B* **1991**, *43*, 1993.
(37) Kleinman, L.; Bylander, D. M. *Phys. Rev. Lett.* **1982**, *48*, 1425.
(38) Souaille, M.; Loirat, H.; Borgis, D.; Gaigeot, M. P. *Comput. Phys. Commun.* **2009**, *180*, 276.

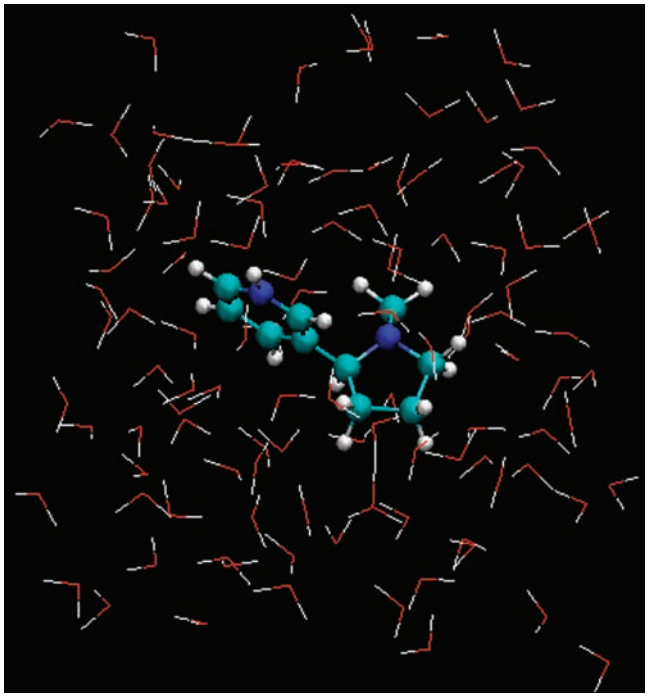

Figure 4. Snapshot of aqueous nicotine from the Car−Parrinello MD simulations performed in the present work. In this figure, the pyridine ring is protonated.

(pyri-dyn) and protonation at the pyrrolidine ring (pyrro-dyn). The solute is surrounded by 111 explicit water molecules, which corresponds to two complete layers of solvent and part of a third one around the solute (Figure 4).

Mean temperatures obtained during the dynamics are 342 ± 13 (pyri-dyn) and 376 ± 14 K (pyrro-dyn), which are appropriate for a correct thermodynamics representation of liquid water when using the BLYP functional within the present CPMD setup.[39] While the protonated nicotine−$(H_2O)_{1-4}$ complex calculations have been performed at the rather high B3LYP/6-311++G(d,p) level in order to evaluate as accurately as possible the proton-transfer energy barriers, we have chosen the BLYP level for CPMD simulations because it provides the best evaluation of the bulk properties. We have also shown in section 2 that BLYP and B3LYP energy barriers were within 8 kJ/mol, and in any case both functionals provided the same energy properties for stationary and transition-state geometries. A CPMD simulation conducted with the B3LYP functional would have required considerably longer computer time.

Proton transfers are rare events that can be very difficult to sample over the time scale of short DFT-based MD (see section 3.2). In order to quantify the free energy of the proton transfer between the two rings of nicotineH^+, we have performed two series of constrained MD. One series investigated the proton transfer between N1 and the solvent, and the other series investigated the proton transfer between N12 and the solvent. The selected constraints were the N1−H and N12−H distances (noted ζ) between the N1 (N12) site of the pyridine (pyrrolidine) rings and the H atom, respectively in each series. ζ was varied between $\zeta_1 = 1.0$ and $\zeta_2 = 2.2$ Å. For each ζ value, a DFT-based MD was performed of 2 ps length (long enough in comparison to the expected proton-transfer time scale) where the force of the constraint was measured. We no longer consider optimized static structures without any constraint as in section 2.1, but rather selected constraints. According to Sprik and Ciccotti,[40] the relative free energy between states ζ_1 and ζ_2 can then be obtained by the following expression:

$$\Delta F = -\int_{\zeta_1}^{\zeta_2} f_{\zeta}' \, d\zeta'$$

where

$$f_{\zeta} = \frac{\langle Z^{-1/2}[\lambda - k_B T G]\rangle_{\zeta}}{\langle Z^{-1/2}\rangle_{\zeta}}$$

is the average force of constraint, k_B is the Boltzmann constant, T is the temperature, and Z and G are factors that compensate for the bias introduced by the constraint (see ref 40 for the full derivation). In the case of a distance constraint as used here, $G = 0$, and $f_{\zeta} = \langle\lambda\rangle_{\zeta}$ is simply the ensemble average of the Lagrange multiplier λ. Lagrange multiplier values have been accumulated over 2 ps DFT-based trajectories, and a standard integration scheme has been applied in order to get ΔF over the $\zeta_1-\zeta_2$ interval.

3.2. Solvation Properties: Structures and Dynamics. 3.2.1. Nicotine Structure and Dynamics. There are two coordinates to be followed along the dynamics of nicotineH^+ in liquid water. The first one describes the motion of the transferred proton between its two preferential sites, the N1 on the pyridine ring and N12 on the pyrrolidine ring. The second one (angle ψ) describes the relative orientation of the two rings of nicotineH^+. We have followed the evolution with time of these two coordinates, as described below. The arrangement of the water molecules in the hydration shells of nicotineH^+ will be described in the subsequent paragraph.

Conformations Pyri-I, Pyrro-I, and Pyrro-II of isolated protonated nicotine were chosen as initial steps in the study of the dynamics of protonated nicotine immersed in liquid water. For each trajectory the protonation site was fixed at the initial time of the simulation. No spontaneous proton-transfer tautomerization of nicotineH^+ took place within the time lengths of the DFT-based dynamics performed here. We thus comment below only on the structural properties of nicotineH^+ in terms of the relative orientation of its rings (angle ψ).

When the dynamics was initiated from the Pyri-I conformation of protonated nicotine, the ψ angle oscillated between 140° and 100° during the simulation time, having a mean value of 122° ± 31°, to be compared to $\psi = 165°$ in the gas-phase optimized structure. With this dihedral angle, the N12 atom of the pyrrolidine ring roughly sat "midway" between the C4 and N1 sites of the pyridine ring, although it had the propensity to be facing the C4 side (average C4−N12 distance of 3.4 Å) more often than the N1 side (average N1−N12 distance of 4.4 Å). Interestingly, the dynamics initiated from the Pyro-II conformation ($\psi = 115°$ in the gas-phase optimized structure) remained in the average orientation for ∼9 ps and then spontaneously evolved toward an intermediate conformation where $\psi \approx 90°$ (during 3 ps). It subsequently drastically changed to a conformation where ψ oscillated between approximately 30° and −10° during the last 6 ps of the dynamics. Concomitantly, the N12−H protonated group evolved from a situation where it faced the N1 side of the pyridine ring to one where it faced the C4 side

(39) Schwegler, E.; Grossman, J. C.; Gygi, F.; Galli, G. *J. Chem. Phys.* **2004**, *121*, 5400.

(40) Sprik, M.; Ciccotti, G. *J. Chem. Phys.* **1998**, *109*, 7737.

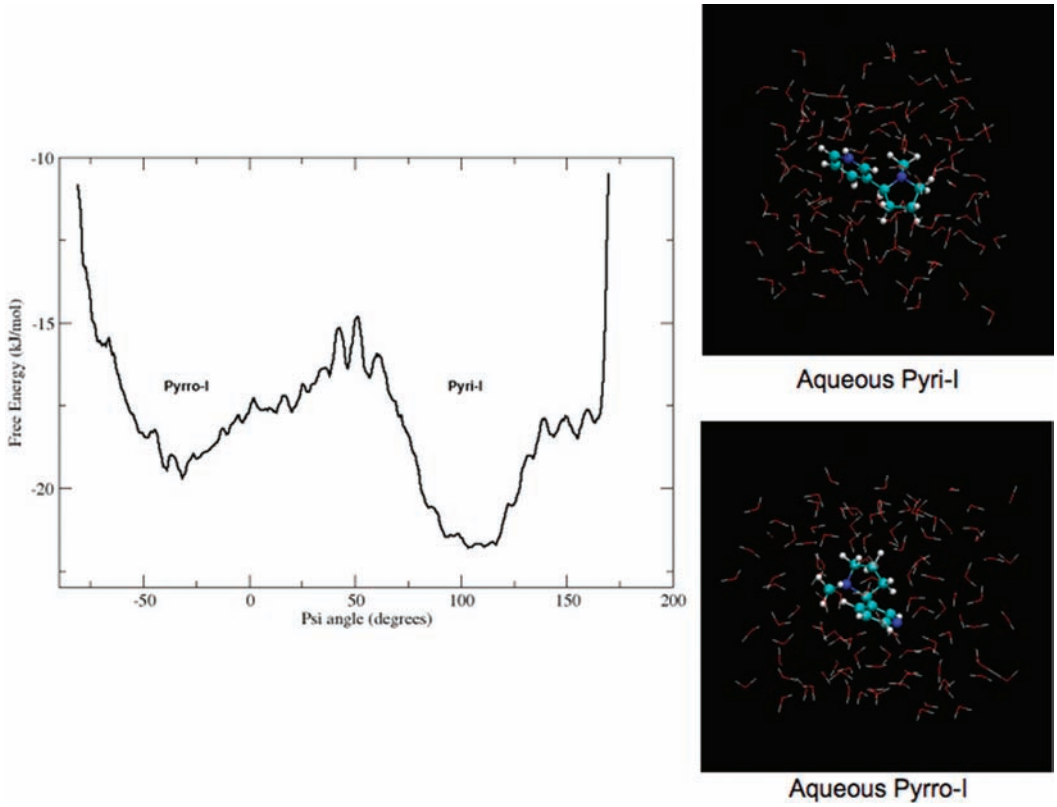

Figure 5. (Left) Free-energy profile along the dihedral angle coordinate ψ = N12−C11−C5−C4 of nicotineH^+ extracted from the DFT-based molecular dynamics simulations in the aqueous phase. ψ is the geometrical coordinate describing the respective orientation of the nicotine rings. For each trajectory the protonation site is fixed, as no spontaneous proton transfer has been observed. The minima in the curve are therefore to be understood in relation with this ψ coordinate only, and they do not correspond to any proton transfer (see text for details). (Right) Snapshots from the dynamics for illustration of typical structures associated with the two wells.

of the ring. The C4−H(−N12) distance typically evolved from 3.5−4.0 to 2.5 Å. There was thus a spontaneous transition from a Pyrro-II conformation to a Pyrro-I conformation (where the average ψ = N12−C11−C5−C4 dihedral angle was close to −30°, see below) in bulk liquid water at room temperature. The Pyrro-II conformation was thus thermodynamically not stable in aqueous solution and instead gave rise to a Pyrro-I-type conformation. There was no conformational transfer back to Pyrro-II within the duration of the dynamics. Conversely, a trajectory initiated from Pyrro-I (ψ = 289° in the optimized gas-phase structure) spontaneously and progressively evolved in liquid water toward a conformation where the dihedral angle ψ was −30° (330°) on average. The average C4−H(−N12) distance was ∼2.7 Å, with the protonated N12−H group facing the C4 side of the pyridine ring.

These conformational dynamics results along the ψ angle coordinate are summarized in Figure 5, where the free-energy profile along the ψ angle coordinate is extracted from the three trajectories generated in the present work. Again we emphasize that for each trajectory the protonation site was fixed, as no spontaneous proton transfer was observed. The minima in Figure 5 are therefore to be interpretated in relation with this ψ coordinate only. The free-energy profile was calculated as $F(\psi) = -kT \ln P(\psi)$, where k is the Boltzmann constant and T is the average temperature of the dynamics. $P(\psi)$ is the probability histogram related to the sampling of the reaction coordinate for the dihedral angle ψ orientation of the pyridine and pyrrolidine rings of nicotineH^+ along the dynamics. $F(\psi)$ displays two main domains that correspond to two broad wells of lower free energies, respectively located at $\psi \approx 110°$ (denoted min-1) and $\psi \approx -30°$ (min-2). Min-2 is broader and shallower than min-1, and as such min-2 is probably entropically slightly more favorable than min-1. These two minima are separated by energy barriers of ∼4.6 kJ/mol (min-1 to min-2) and ∼0.6 kJ/mol (min-2 to min-1). Such weak free-energy barriers are easily overcome at room temperature, as indeed it has been sampled during our dynamics. Note that the free-energy well min-1 centered on $\psi \approx 110°$ represents nicotineH^+ structures that can be protonated either at the N1 site (pyridine ring) or at the N12 site (as observed with the transient Pyrro-II conformations), whereas the free-energy well min-2 centered on $\psi \approx -30°$ is related only to conformations protonated at the N12 site (pyrrolidine ring). These low free-energy barriers between the two wells will most probably be necessary once the proton transfer between the two rings occurs, as this will undoubtedly help the necessary subsequent conformational rearrangements. This will be further discussed in section 3.3.

In conclusion, aqueous nicotineH^+ adopted two major relative orientations of its rings in the liquid phase, i.e., Pyri-I with ψ = 110° when the protonation occurred at the N1 (sp^2) site and Pyrro-I with $\psi \approx -30°$ (330°) when the protonation was at the N12 (sp^3) site. The Pyrro-II conformation was not thermodynamically stable in the liquid phase. Considering these dihedral angles, Pyri-I corresponded to conformations where the N12 atom was on average placed midway between N1 and C4 sites of the pyridine ring, although it had a higher propensity to face the C4 side, whereas the N12−H group of Pyrro-I definitely faced the C4 side of the pyridine ring and thus away from the N1 site.

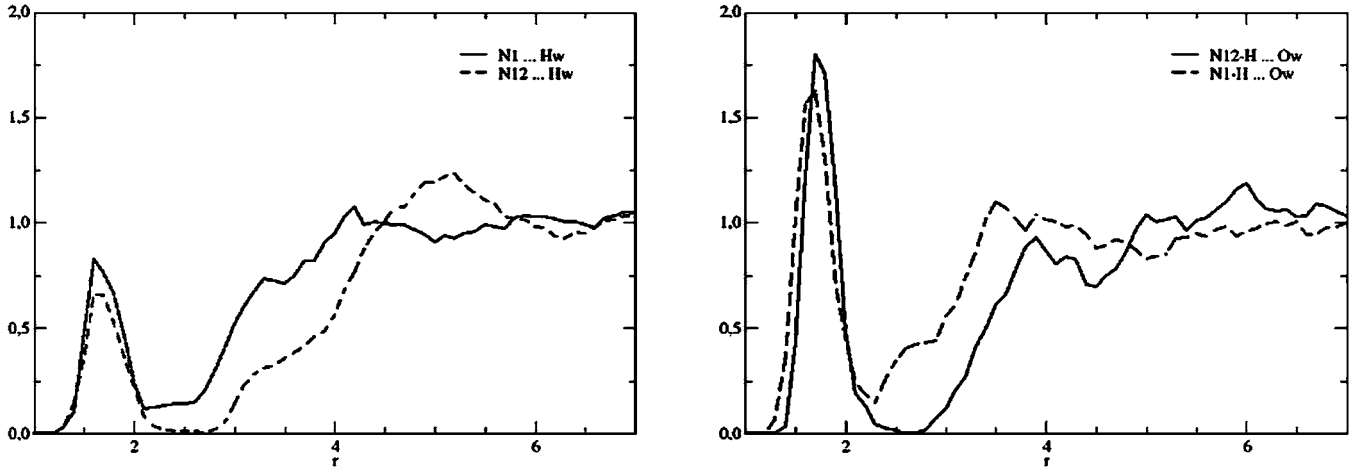

Figure 6. Radial distribution functions (RDFs) of N···Hw (left) and N−H···Ow (right) solute−solvent atom pairs from DFT-based molecular dynamics. N1···Hw (left) goes with N12−H···Ow (right) in Pyrro-I conformations, and N12···Hw (left) goes with N1−H···Ow (right) in Pyri-I conformations. Pair distances r are in angstroms.

Consequently, the nicotineH^+ conformations encountered in the liquid phase have relative orientations of the two rings that are not favorable *by construction* to the direct proton transfer from one N site to the other, since these nitrogen atoms do not face each other. In the following text, we will keep the names Pyri-I and Pyrro-I for the thermodynamically stable conformations of aqueous nicotineH^+, keeping in mind that the average relative orientation of the two rings now corresponded to $\psi \approx 110°$ (min-1, aqueous Pyri-I) and $\psi \approx -30°$ (min-2, aqueous Pyrro-I) when the molecule was immersed in liquid water.

Let us comment on the differences observed in the values of the angle ψ between the liquid-phase simulations and the optimized structures, including up to four water molecules (section 2). ψ is typically 133° and 159° for pyri-1-a and pyri-1-b, respectively, and 109° for pyri-4-a structures. There was thus a decrease of the value of this angle with the inclusion of additional water molecules complexed to pyri-nicotineH^+. Adding a continuum to the complex did not change these results. Remarkably, Pyri-4 optimized structures of nicotineH^+−$(H_2O)_4$ displayed a ψ angle close to the value obtained when nicotine is immersed in bulk water. In contrast, the aqueous structure of Pyrro-nicotineH^+ was totally different from the one complexed with four water molecules. In particular, in the bulk, nicotine protonated on the pyrrolidine ring had on average its N12 site facing the C4 site of the pyridine ring, as described above. This is not the case for nicotine surrounded by four waters only. Adding a continuum did not provide the proper microscopic view either. The influence of the full bulk water is thus pivotal in order to get a complete view of solvation of this isomer.

3.2.2. Solvent Organization. The structural analysis of the water solvent organization was performed by using radial pair distribution functions (RDFs) as is usual in simulations of liquids. They provided an overview of the hydrogen-bonding pattern among the solvent molecules and between the solute hydrophilic groups and the solvent. The relevant RDFs are reported in Figure 6, respectively for N···Hw and N^+−H···Ow pairs (hereafter, water oxygen atoms are denoted by Ow and water hydrogen atoms by Hw; labeling of the nicotine atoms is still taken from Figure 1). RDFs of C−H···Ow, C−H2···Ow, and C−H3···Ow groups can be found in the Supporting Information as well as the RDFs of the aqueous solvent. These latter ones were identical for all three simulations performed here and were identical to our previous investigations of different solutes immersed in bulk liquid water with DFT-based Car−Parrinello dynamics.[31,41,42] They thus corresponded to the expected conformational H-bonded features of liquid water at ambient temperature. This validates our choice of box size and number of water molecules in the simulation cell for a proper representation of liquid solvent at room temperature around this "bulky" solute molecule. The first peaks in the RDFs were found roughly located in the range 1.5−2.5 Å and corresponded to hydrogen bonds that were formed between the pair of atoms considered (water−water or solute−water). The second peaks were located at longer distances of about 3.5−5.0 Å, corresponding to pairs of atoms located in the second hydration shell.

The broad picture of the hydration properties of nicotineH^+ emerging from the present CPMD simulations follows the general trends usually encountered for organic molecules. Hence, N···Hw and N^+−H···Ow RDFs display a clear first peak at distances ca. 1.60−1.80 Å that correspond to water molecules being hydrogen-bonded to the N and N^+−H sites of nicotineH^+. The C−H(1,2,3)−Ow RDFs had a first peak located at much larger distances of about 3.5 Å. This peak corresponds to water molecules located in the hydrophobic environment of the CH, CH_2, and CH_3 groups of the solute. As can be observed in Figure 4, those molecules are not engaged into any hydrogen bonding with these groups. More precisely, as can be seen from N−Hw RDFs (respectively N12−Hw for Pyri-I and N1−Hw for Pyrro-I, Figure 6), the nicotine non-protonated sites were involved in hydrogen bonding with the surrounding water molecules, with the first peak in the RDFs located at a very short distance, ca. 1.60−1.70 Å, and slightly shifted depending on the protonation site and internal conformation (as defined by angle ψ) of nicotineH^+. The position of the second peak revealed that the second hydration shell around the non-protonated N atom is located at a much shorter distance (4 Å) for the pyrrolidine protonated molecule (N1(sp^2) accessible site) than for the pyridine protonated molecule (5 Å, N12(sp^3) accessible site). This is due to the CH hydrophobic environment surrounding the N12 site. The hydration shells of water molecules around the protonated N^+−H site of nicotine are composed of strongly (see the higher amplitude of the first peak) H-bonded water molecules located at 1.70 Å for

(41) Gaigeot, M. P.; Vuilleumier, R.; Sprik, M.; Borgis, D. *J. Chem. Theory Comput.* **2005**, *1*, 772.
(42) Gaigeot, M. P. *J. Phys. Chem. B* **2009**, *113*, 10059.

Pyri-I and a second hydration shell that is located in the 3.5−4.2 Å range. The N^+−H−Ow RDF of the Pyrro-I conformation of nicotineH^+ displays very similar features, with the same first peak and a second solvation shell pushed slightly farther away (in comparison to Pyri-I), at 3.9−4.5 Å.

The well-defined first peaks in the N−Hw and N^+−H−Ow radial distributions can be used to estimate the effective number of hydrogen bonds formed by these polar groups. Hence, if we take the integral of the curves up to the minimum at $r_{min} \approx$ 2.40−2.50 Å (which corresponds to the conventional maximum bond length of H-bonds), we find that the non-protonated N atom has a coordination number of 1.0 on average for Pyri-I (N12, sp^3) and Pyrro-I (N1, sp^2) and thus forms a single hydrogen bond with water on average. The usual way to estimate the "relative strength" of the H-bond network between solute and solvent in condensed-phase simulations is to compare values of RDF_{max}/RDF_{min} (ratio of RDF amplitudes taken at the position of the maximum and minimum of the first peak). These ratios have no unit and are compared to each other. Although they cannot be used to define bond strengths (there are no hydrogen bond energetics associated with the definition; the definition is based only on distances), they can be used to compare the behavior of hydrophilic groups toward H-bond formation. Hence, a high value of the RDF_{max}/RDF_{min} ratio signifies that water molecules are strongly attracted by the hydrophilic site, while a low value of the ratio signifies the opposite. Values are compared to each other and to those obtained for water−water hydrogen bonds. The values for the N···Hw H-bonds were found to be equal to 70 and 6, respectively for Pyri-I and Pyrro-I. As a comparison, RDF_{max}/RDF_{min} was equal to 7 for the water−water H-bond in the liquid. As a consequence, the N12 sp^3 nitrogen thus strongly attracted with water molecules in its vicinity, while this attraction was far less important with the N1 sp^2 site and is comparable to water−water H-bonds. The N^+−H hydrogen atom of the protonated site has a coordination number of 1.0 both for Pyri-I and Pyrro-I conformations, on average. The RDF_{max}/RDF_{min} ratios for the N^+−H···Ow H-bonds are 11 and 70, respectively, for Pyri-I and Pyrro-I, again to be compared to 7 for Ow···Hw H-bonds.

We thus find that the N12 site always strongly attracts water molecules in order to form H-bonds with the solvent, whether it is protonated (Pyrro-I) or not (Pyri-I). The direct consequence is that it is more favorable to form N12···Hw or $N12^+$−H···Ow H-bonds rather than water−water H-bonds around that site; in other words, water molecules will preferentially organize into direct H-bonds with the solute at that site rather than keeping the bulk water−water H-bonding patterns. Overall, the relative H-bonding features obtained in these simulations give $N12^+$−H···Ow (Pyrro-I) = N12···Hw (Pyri-I) > $N1^+$−H···Ow (Pyri-I) > Hw···Ow > N1···Hw (Pyrro-I) (where the sign ">" means more favorable for the formation of H-bonds with water molecules and "=" means equally favorable).

3.2.3. Solvent Bridges. We have analyzed the trajectory of conformers Pyri-I and Pyrro-I in liquid water further in terms of possible water molecules bridging the two nitrogen sites of nicotineH^+. Quantum calculations at 0 K presented above dealt with nicotineH^+ H-bonded to a few water molecules that were organized into a bridge directly established between the two available protonated sites. It is therefore pivotal to investigate whether formation of those bridges also occurred when the solute was immersed in the bulk liquid solvent at finite temperature. This is an intriguing question, as solvation always results from the balance between solute−water and water−water interactions. One could imagine (see a related discussion in ref 32) a compromise between inserting the solute within the solvent without too much perturbation of the surrounding solvent−solvent H-bond network and stabilizing the solute within the bulk by forming solute−solvent H-bonds that very slightly disrupted the local solvent−solvent H-bond network. Judging by the H-bond forces derived above for Pyri-I, $N1^+$−H···Ow is energetically roughly equivalent to Ow···Hw H-bonds, whereas N12···Hw is much stronger than Ow···Hw. In the case of Pyrro-I, N1···Hw is roughly equivalent to Ow···Hw H-bonds, while $N12^+$−H···Ow is much stronger than Ow···Hw. The local organization of the bulk solvent between the two nitrogen sites will therefore reflect these extreme values of the solute−solvent forces.

We find that the water molecules " linked " to N1 on the pyridine and to N12 on the pyrrolidine ring were organized into H-bonded bridges between the two available N sites of nicotine. Bridges are defined as follows in the dynamics: two H_2O molecules are considered as hydrogen-bonded when the Ow···Ow distance is shorter than 3.5 Å, in agreement with the first minimum position in the corresponding RDF of the bulk water (see Supporting Information). According to the solute−solvent RDF discussed above, a water molecule is considered H-bonded to the N or $N^{(+)}$−H atom if N···Hw or $N^{(+)}$−H···Ow < 2.5 Å. We have not applied any additional criteria about H-bond angles in our analysis. Considering that the organization of the first hydration shell around nicotineH^+ is the result of a compromise between solute−solvent and solvent−solvent interactions, these chain water molecules will, at best, form a strained water−water H-bond network, so that optimal values for the H-bond angle (typically >150°) cannot be easily achieved. We have in fact found that H-bond criteria applied on both Ow···Ow distances and Ow−Hw···Ow angles are too much restrictive, and the formation of water H-bonded bridges between the two protonation sites of nicotineH^+ would then be unlikely. We have also analyzed the bridges in terms of number of water molecules involved, mainly differentiating bridges composed of two, three, or four water molecules.

Water bridges composed of three or four water molecules can be observed for a total duration of about 8 ps over the dynamics of Pyri-I (nicotineH^+ protonated on the N1 pyridine ring) with alternate events of three/four water bridges, but bridges composed of only two water molecules never occur along the dynamics. The average lifetime of the water bridges is about 300 fs (bridges of four water molecules having slightly longer lifetimes), with also longer periods of 1 ps. Such bridges do exist over half of the trajectory. The rather short lifetime obtained here reveals the dynamical behavior of the bridges, which easily break and (re)form at finite temperature. The existence of these bridges for 50% of the trajectory length demonstrates their high probability. The dynamics of Pyrro-I reveals that bridges composed of three water molecules are the most likely to be formed, for a total duration of about 4 ps over the trajectory. No bridges composed of two or four water molecules have been observed within the time of the simulation.

Overall, we thus find that protonation on the pyridine site is more favorable to give rise to water bridges forming a chain between N1−H and N12, with chains composed of four water molecules being the most stable. Illustrations of the water chains are presented in Figure 8 (below) in the special case of the proton-transfer mechanism. We will indeed see in the next section how these bridges might play a role in the proton transfer between the two rings of nicotineH^+ in the aqueous phase.

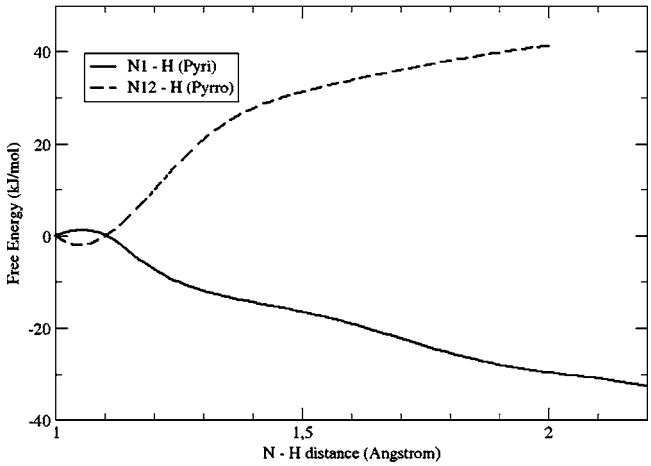

Figure 7. Free-energy profiles for the proton transfer between N1 (solid line) or N12 (dashed line) of nicotineH^+ and the aqueous solution calculated from biased DFT-based MD. See text section 3.1 for more details. The N1(N12)···H distances are reported in angstroms and free energy in kJ/mol. The zero of energy has been taken at a distance N1(N12)···H equal to 1.0 Å for each energy curve.

3.3. Proton Transfer in Bulk Liquid Water. As observed in section 3.2, no spontaneous tautomerization of nicotineH^+ was observed within the time of the dynamics performed in our work. Biased MD are therefore necessary to assess the energetics and mechanisms of this proton-transfer process in bulk liquid water. See section 3.1 for details on the two series of constrained dynamics performed. The first information from these trajectories is contained in the free-energy profile for the proton transfer from the preferential gas-phase $N1^+$−H site of nicotineH^+ to the surrounding solvent, as presented in Figure 7 (solid line). By going from distance $N1^+$−H equal to 1.0 Å to 2.2 Å, there is first a small energy barrier of about 1.25 kJ/mol to overcome at a distance of about 1.05 Å before the proton is released into the water solvent. The free energy subsequently steadily decreases up to the maximum distance sampled at 2.2 Å. Note that when the distance N1−H is equal to 1.2 Å, the proton is still in the vicinity of the N1 atom, forming a long hydrogen bond with it. When this distance increases to 2.0 Å, the proton is part of a hydronium H_3O^+ ion immersed in liquid water at the initial step of the dynamics. When such a condition is reached, we subsequently observed proton transfers taking place within the liquid until a path is found leading to the reprotonation of the nicotine molecule at the pyrrolidine ring. We observed that the reprotonation at the pyrrolidine ring could occur only when one H_3O^+ ion had been formed in the aqueous solution (for N1−H = 2.0 Å here). All biased dynamics performed with intermediate values of the N1−H constrained bond length never led to proton transfers in the liquid nor to reprotonation of the pyrrolidine ring, at least within the time scale of the constraint dynamics performed here.

The small barrier and subsequent decrease of the free-energy profile indicate that there is indeed an energetic preference for aqueous nicotine to be deprotonated at the pyridine site. The preference for the proton to be located at the N12 pyrrolidine site is confirmed by the free-energy profile obtained from constrained MD, where N1 is now held deprotonated and N12−H bond length is varied between 1.0 and 2.0 Å in the constrained MD (Figure 7, dashed curve). There was indeed a net decrease in the free energy for the proton to go from the solvent to the N12 site of nicotine, in contrast to the profile obtained for the N1 site.

Gains of 30−40 kJ/mol in free energy were obtained through these processes (proton transfer from N1 to the solvent or proton transfer from the solvent to N12), in perfect agreement with the experimental observations.[7] Note that nuclei quantum effects generally decrease the values of barriers for proton transfers (see for instance ref 18).

The second information provided by the constraint dynamics is that the deprotonation (Pyri)−reprotonation (Pyrro) process of nicotine is very fast, occurring in less than 0.5 ps in the constraint dynamics performed here. The protonation immediately gives rise to a conformational change of nicotineH^+. Angle ψ decreased from the 120° value typical of Pyri-I in liquid water to a value of 90−100°, which was maintained on average during the 5 ps dynamics performed after the reprotonation event at the N12 site took place. With that dihedral orientation, the N12−H group was sitting midway between the N1 and C4 sides of the pyridine ring, with average N12−H···N1 and N12−H···C4 distances respectively of 3.9 and 3.6 Å. Considering the free-energy curve displayed in Figure 5, crossing the barrier to reach $\psi \approx -30°$ of Pyrro-I is possible at room temperature, and continuing the dynamics will lead to a final conformation change into a Pyrro-I kind of structure, as expected with protonation on the N12 atom.

The third pivotal information provided by the biased MD simulations is that the proton transfer proceeded through the water chain bridging N1−H and N12 sites of nicotine. This is illustrated by the snapshots in Figure 8. We have already mentioned that these four water chains are present with a high probability when protonation occurs at the pyridine ring (N1−H) (see nonconstrained dynamics reported in section 3.2). These results further demonstrate that these water bridges can be used as a path to promote the proton transfer between the two nitrogen sites (and two rings) of nicotine immersed in bulk liquid water.

Proton transfers are rare events, which can remain elusive in MD simulations, especially in rather short *ab initio* dynamics. The nonbiased dynamics performed in this work (section 3.2) did not show that these events occur spontaneously. Thermal and/or dynamical fluctuations usually trigger these rare events, presumably not encountered during the time of the nonbiased MD. Note that a nonconstrained dynamics initiated with N1−H bond length longer than 1.5 Å led to the release of the proton into the solvent within less than 1 ps of trajectory.

The choice of the reaction coordinates for the biased MD simulations has to be discussed. The choice of N1−H and N12−H distances as constraints in separate series of constrained MD is simple enough for the simulations but provides two separate free-energy profiles. This situation does not allow the extraction of the free-energy profile of the double proton transfer, i.e., deprotonation of the pyridine ring and reprotonation of the pyrrolidine ring process in one unique series of constrained MD. Our choice provides only the energetics for each step of the double-proton process. The double-proton-transfer free-energy profile could have been obtained by using more complicated reaction coordinates, as in ref 43. Nonetheless, the free-energy profiles extracted from our dynamics clearly show that the deprotonation of the pyridine ring is an almost barrier-less process when nicotine is immersed in liquid water. This is a clear indication that the tautomerization process can be easily achieved once nicotineH^+ is solvated by bulk water, in agreement with experimental observation.[7] Subsequent reprotonation

(43) Burisch, C.; Markwick, P. R. L.; Doltsinis, N. L.; Schlitter, J. *J. Chem. Theory Comput.* **2008**, *4*, 164.

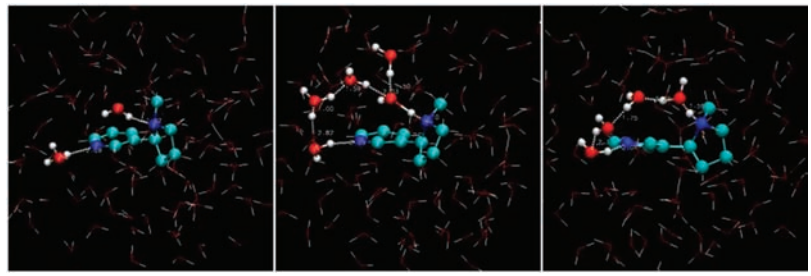

Figure 8. Snapshots from the biased DFT-based MD simulation illustrating the proton transfer between the protonated pyridine site (left, Pyri I) to the protonated pyrrolidine Pyrro I or II site (right). (Left) H_3O^+ ion H-bonded to N1 and H_2O H-bonded to N12; other water molecules that form the water bridge from N1 to N12 have not been highlighted. (Middle) A typical situation where a bulk hydronium ion is formed as an intermediate species within the water chain bridging N1 to N12 sites of nicotine along the proton transfer. (Right) Protonation of N12 after the proton transfer has been achieved, with deprotonated N1 H-bonded to one water molecule of the bulk. Again, other water molecules that form the water bridge from N1 to N12 have not been highlighted. In all figures, H-bond distances are shown for illustration.

of nicotine at the N12 site is very fast, achieved through the proton hopping along the water molecules that bridge N1 and N12 sites in the bulk. We can estimate gains in free energy of roughly 30−40 kJ/mol through the whole process.

4. Conclusion

Determination of accurate structures and energy barriers between different protonation sites of hydrated complexes of nicotine has provided the following relevant information about the proton transfer between the inactive and active forms of nicotineH^+: (1) Once three water molecules are H-bonded between the two protonation sites (N1 on the pyridine and N12 on the pyrrolidine ring), conformations protonated on N12 become energetically favorable. (2) The free-energy barrier of the minimum-energy path for the proton transfer decreases from 300 kJ/mol in the gas phase to 16 kJ/mol when four water molecules are H-bonded to nicotineH^+. A single water molecule belonging to the "second-solvation shell" plays an important role in the decrease of the free-energy barrier.

The DFT-based molecular dynamics of nicotineH^+ immersed in liquid water (111 explicit water molecules taken into account in the present simulations, i.e., two complete solvation layers supplemented by part of the third layer) have shown that the proton transfer from the inactive form (pyri-type of conformation) to the active form (pyrro-type of conformation) of nicotine occurs barrierless. These simulations have been conducted at a biologically relevant temperature. In bulk water, short-lived water bridges established between N1 and N12 sites of nicotine, involving a rather small number of water molecules (3−4), were shown to assist the proton movement. Those water bridges easily form through temporary formation of hydronium ions and break on a sub-picosecond time scale.

This work has provided two very complementary views of the proton-transfer tautomerization of nicotineH^+: one from static calculations, which included up to four water molecules complexed with nicotine, possibly supplemented by a continuum solvent, and one from statistical mechanics, which included temperature and full microscopic solvent. Although both methods have shown that the proton transfer occurs through a water network that bridges the N1 and N12 sites of the solute, the very nature of the bridge is totally different in both calculations. In the bulk, the bridge is indeed part of the 3D water−water H-bond network; i.e., it remains embedded within the bulk. This property is probably the reason why the energy of the barrier for the proton transfer disappears. Whereas a barrier of 16 kJ/mol for the proton transfer could still be overcome when four water molecules were in complex with nicotine, the proton transfer is barrierless once nicotine is immersed in liquid water. Interestingly, the presence of a continuum water solvent increased the free energy of the barrier for the tautomerization process. The microscopic nature of the bulk appears mandatory for a proper account of the tautomerization process of nicotine.

It may seem that the very local picture of the interaction of a single nicotine molecule with its water surroundings presented here is quite far from the binding of the drug to the large AChR receptors. In fact, the very local microenvironment of nicotine is crucial. Nicotine protonated on its pyrrolidine site strongly binds to a single specific tryptophan amino acid (called TrpB, residue 149) of its different receptors through a cation−π interaction. A recent work has demonstrated that the subtle enhancement of a hydrogen bond from nicotine to the backbone carbonyl of TrpB is sufficient to explain why (fortunately) brain and muscle receptors behave differently and smoking does not lead to insufferable contractions.[1] It may be that an explicit treatment of water in the very local microenvironment of nicotine and crucial binding sites of its receptor within the very first hydration layers can provide the essential features of the interaction between the drug and its receptors.

Acknowledgment. The authors acknowledge the reviewers for their valuable comments and Prof. E. Kunji from the MRC-Cambridge for his critical reading of the manuscript. The authors thank IDRIS (Orsay, France) for a generous allowance of computer time. This work was performed using HPC resources from GENCI-IDRIS (Grant 2009-i20080712484). A.C. acknowledges a post-doctoral fellowship from Genopole-France (ATIGE program). M.P.G. acknowledges Churchill College, Cambridge, UK, and the French Foreign Office for the allowance of an Overseas Fellowship in 2008 and 2009. J.P.S. thanks the support of this work by grant No. R31-2009-100320 from the World Class University (WCU) project of the Ministry of Education, Science & Technology (MEST) and the National Research Foundation of Korea (NRF) through Seoul National University. S.L. thanks the Ministry of Education, Science and Technology (Converging Research Program, No. 2010K001203) and the Ministry of Health, Welfare and Family affairs of Korea for financial support.

Supporting Information Available: Nicotine−$(H_2O)_{n=1-4}$ complex calculations and Car−Parrinello molecular dynamics simulations; complete ref 22. This material is available free of charge via the Internet at http://pubs.acs.org.

JA103759V